Assessing the Efficiency of the Air Isolation System Based on the Mathematical Models

Zhihong Zhou

Xinjiang Shihezi Vocational Technical College, Skills Training Branch, Shihezi, China.
Sanfeng Intelligent Equipment Group Co., Ltd, Huangshi, China.

Huichuan Xu

Sanfeng Intelligent Equipment Group Co., Ltd, Huangshi, China.

Vanliem Nguyen, Lijing Pan and Binbin Wang

School of Mechanical and Electrical Engineering, Hubei Polytechnic University, Huangshi, China.

Two calculation methods of the lumped parameter model (LPM) and mass flow ratio (MFR) used to establish dynamics models of air isolation system (AIS) in vehicles are widely applied. However, the efficiency and application range of the LPM and MFR for the AIS of the vehicles have not been explained in detail. To clarify this issue, the numerical simulation and experiment of the AIS performed under the harmonic excitation are given to evaluate the accuracy of the LPM and MFR. The two-axle automobiles and multi-axle heavy trucks equipped with the AIS are also simulated to evaluate the efficiency of the AIS with the LPM and MFR in improving ride comfort and road friendliness. The study shows that with the single model of the AIS, measured and simulated result in AIS's force response, force-deformation characteristic, and dynamics stiffness-frequency characteristic with LPM and MFR are similar. Therefore, both methods could be applied to establish the dynamic model of the AIS. However, by applying the AIS on the two-axle and multi-axle vehicles, the MFR improves road-friendliness and comfort in two-axle automobiles better than the LPM, conversely, the LPM improves road-friendliness and comfort in multi-axle trucks better than that the MFR. Therefore, to more accurately assess the isolation efficiency of the AIS in improving road-friendliness and comfort in vehicle, the MFR should be applied to the AIS using the pipe designed by the parallel pipes or long pipes of two-axle vehicles whereas the LPM should be applied to the AIS using the pipe designed by the complex pipes of multi-axle vehicles.

1. INTRODUCTION

To enhance moving quality and reduce road damage in vehicles equipped with passive isolation systems using steel or leaf springs, the vehicle's passive isolation systems had been researched by restoring the air-isolation-systems (AIS) or controlled isolation systems.[1–5] For further enhancing comfort in the vehicle, the operation parameters of the AIS were then optimized and applied on vehicles.[6–9] The research results showed that with the vehicles using the AIS, both road friendliness and comfort in vehicles were ameliorated under different operating conditions, especially under the vibration excitations lower than 10.0 Hz.[6, 10]

With the AIS equipped on the vehicles, its structure was designed by the airbag chamber, the auxiliary chamber, and the pipe. The airbag chamber was connected with the auxiliary chamber via the pipe.[3, 4, 11–13] To evaluate the isolation efficiency of the AIS, based on the thermodynamic theory, the structure and design parameters of the AIS were researched and analyzed via the characteristics of the force response-time, force-deformation, and force-frequency of the airbag chamber.[14, 15] The experimental study of the AIS was also performed to validate the results of theoretical research.[11, 12, 16–18] Based on the published papers on the AIS in the existing studies, we find that there are two different computational methods used to establish AIS's dynamics models as follows:

(1) Method of the lumped parameter model (LPM): From AIS's actual design parameters and thermodynamic theory, the dynamic parameters of the elastic stiffness, damping coefficient, static stiffness, and mass of the air in the pipe were calculated to establish the AIS's dynamic model.[1, 4, 18–20] The studies showed that this method could independently evaluate the influence of the elastic stiffness, static stiffness, and damping coefficients of the AIS using complex pipes. Concurrently, these parameters were easily optimized to enhance the isolation efficiency of the AIS. This method was then mainly applied to the AIS of multi-axle vehicles (trains and heavy trucks) to ameliorate the road-friendliness and comfort.[5, 21, 22] (2) Method of the mass flow rate (MFR): Based on the thermodynamic theory and the ratio of the air's mass-flow to airbag chamber, pipe, and auxiliary chamber of the AIS, the dynamic stiffness was then determined to establish the AIS's dynamic model and evaluate its isolation efficiency.[23–26] The studies showed that this method is simple for establishing the model and calculating the dynamic characteristics of the AIS using parallel pipes or long pipes.[2, 16] Concurrently, the resisting force of flow in the pipe was also determined based on the equation of the rate of the air's mass flow rate via the pipe. Then, this method had been mainly applied for AIS in two-axle vehicles of the ambulances and cars to ameliorate the stability and comfort.[23, 24, 26]

Both methods of the LPM and MFR for the vehicle's AIS

were widely applied in the existing studies. Experimental research was also performed to evaluate the accuracy of the LPM and MFR.[6,18,23,24] However, the comparison of the efficiency between the two methods of the LPM and MFR as well as the application range of each method for the AIS of the vehicles have not been evaluated and highlighted in detail. To clarify this issue, the numerical simulation and experiment of the AIS performed under the harmonic excitation are given to evaluate the accuracy of the LPM and MFR. The two-axle automobiles and multi-axle heavy trucks equipped with the AIS are then simulated to evaluate the efficiency of the AIS with the LPM and MFR in improving ride comfort and road friendliness. The objective study is to elucidate the isolation efficiency of the AIS using the two methods of the LPM and MFR as well as the application scope of the two methods for the AIS of the different vehicles.

2. MODELING OF AIR ISOLATION SYSTEM

The AIS was designed by an airbag chamber connected with an auxiliary chamber via the pipe,[4,10–13,22] as shown in Fig. 1a. Where, z and x_p were the deformation of the airbag in the vertical direction and air displacement in pipe; A and A_p were the effective area of airbag and section area in pipe; V and V_a were the volumes of the airbag and auxiliary chambers; p and p_a were the pressures of the airbag and auxiliary chambers; m_p and l_p are the air mass in pipe and pipe's length, respectively.

To determine the dynamic characteristic and the stiffness parameter of the AIS, two methods of the LPM and MFR were directly used as follows.

2.1. Method of Lumped Parameter Model (LPM)

From the model of the AIS in Fig. 1a, the LPM method[1,4,10,11,22] was used to determine the deformation-force characteristic and dynamic stiffness of the AIS as follows.

Under the impaction of the force F', the force response (F) generated by the pressure in the airbag chamber was calculated as:

$$F' = F = A(p - p'_a);\tag{1}$$

where p'_a was the standard atmospheric pressure.

To determine the p, both the V and p of the airbag chamber need to be calculated via V_a and p_a of the auxiliary chamber as:[4,12]

$$\begin{cases} V = V_0 - Az + A_p x_p; \\ V_a = V_{0a} - A_p x_p; \end{cases} \quad \text{and} \quad \begin{cases} p = p_0 + \Delta p; \\ p_a = p_0 + \Delta p_a; \end{cases}\tag{2}$$

where V_0 and V_{0a} were the initial volumes of the airbag and auxiliary chambers; Δp and Δp_a were the pressure changes of the airbag and auxiliary chambers; p_0 was the initial pressure of the AIS.

Based on the general equation between the volume and pressure at two different status with a polytropic constant of γ expressed by $p_0 V_0^\gamma = p V^\gamma$, thus, the relation between the volumes and pressures in the airbag and auxiliary chambers in Eq. (2) was calculated by:

$$\begin{cases} p_0 V_0^\gamma = (p_0 + \Delta p)(V_0 - Az + A_p x_p)^\gamma; \\ p_0 V_{0a}^\gamma = (p_0 + \Delta p_a)(V_{0a} - A_p x_p)^\gamma. \end{cases}\tag{3}$$

Based on the calculation result given by Robinson,[24] both values of Δp and Δp_a in Eq. (3) were then determined by:

$$\begin{cases} \Delta p = \frac{\gamma(Az - A_p x_p)}{V_0} p_0; \\ \Delta p_a = \frac{\gamma A_p x_p}{V_{0a}} p_0. \end{cases}\tag{4}$$

By substituting Δp in Eq. (4) and p in Eq. (2) into Eq. (1), the force equation was written as

$$F = \left[\left(\frac{\gamma A}{V_0} z - \frac{\gamma A_s}{V_0} x_p + 1 \right) p_0 - p'_a \right] A.\tag{5}$$

Under the effect of the force F', the balancing force conducted by moving air in the pipe was calculated by:[1]

$$m_p \ddot{x}_p = (\Delta p - \Delta p_a) A_p - c_p \dot{x}_p^\delta.\tag{6}$$

By substituting Δp and Δp_a in Eqs. (4) to (6), the F in Eq. (5) and the balancing force in Eq. (6) were written as:[12,24]

$$F = (p_0 - p'_a)A + k_s z + k_v(z - x);\tag{7}$$

$$m\ddot{x} = k_v(z - x) - c_p k^{1+\delta} \dot{x}^\delta;\tag{8}$$

where c_p was the damping coefficient of the flow determined by $c_p = 0.5 A_p \rho_p (c_f + c_e + c_c + c_b)$; c_f, c_c, c_e, and c_b were the loss coefficients due to the friction, contraction, enlargement, and bends in the pipe; $m = k^2 m_p$; $m_p = \rho_p A_p l_p$; $k = AV_{0a}/(V_0 + V_{0a})A_p$; $k_v = k_s V_{0a}/V_0$; $k_s = \gamma p_0 A_2/(V_0 + V_{0a})$; $x = x_p/k$; $\gamma = 1.34$; ρ_p was the density of the air in the pipe.

Observing Eq. (7), we can see that under the impaction of the force F, three different forces of the AIS exist including the static load of $F_{sl} = (p_0 - p'_a)A$, the static force of $F_{st} = k_s z$, and the viscous force of $F_{vf} = k_v(z - x)$.

In addition, based on the calculation results given by Presthus,[1] Ni, et al.,[10] and Berg,[11] the viscous force of $F_{vf} = k_v(z - x)$ was also determined via the velocity over the damper c_δ as:

$$F_{vf} = k_v(z - x) = m\ddot{x} + c_\delta |\dot{x}|^\delta \text{sign}(\dot{x}) \quad \Rightarrow$$
$$\Rightarrow \quad m\ddot{x} = k_v(z - x) - c_\delta |\dot{x}|^\delta \text{sign}(\dot{x}).\tag{9}$$

It can see that the damping force in Eqs. (8)–(9) was equivalent, thus, the relation between c_p and c_δ was determined by:

$$c_\delta = c_p k^{1+\delta}.\tag{10}$$

Therefore, the lumped parameters including k_s (static-stiffness coefficient), k_v (viscous-stiffness coefficient), c_δ (damping coefficient), and m (air mass in pipe) were calculated based on the initial parameters of the AIS were rewritten by:

$$\begin{cases} k_s = \frac{\gamma p_0 A^2}{V_0 + V_{0a}}; \\ k_v = k_s \frac{V_{0a}}{V_0}; \end{cases} \quad \text{and} \quad \begin{cases} c_\delta = c_p \left(\frac{V_{0a}}{V_0 + V_{0a}} \frac{A}{A_p} \right)^{1+\delta}; \\ m = \rho_p A_p l_p \left(\frac{V_{0a}}{V_0 + V_{0a}} \frac{A}{A_p} \right)^{1+\delta}. \end{cases}\tag{11}$$

Based on the calculation result of the lumped parameters of the AIS in Eq. (11), the mathematical model of the AIS using the LPM method is described in Fig. 1b.
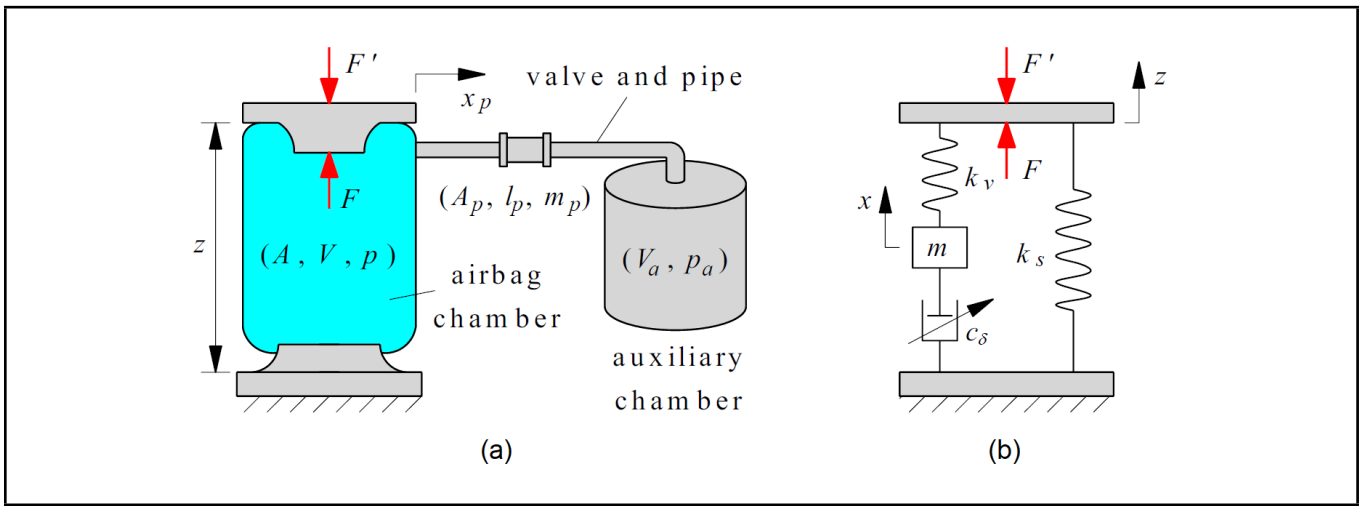
Figure 1. The model of the AIS (a) and LPM of the AIS (b).

2.2. Method of Mass Flow Rate (MFR)

In the existing studies of the car's air isolation system,[21,23,24] another method of the MFR was also used to compute the dynamic stiffness and characteristic of the AIS based on the model of the AIS in Fig. 2a. Where Q was the mass flow rate in the AIS; ρ, ρ_p, and ρ_a were the air density in the airbag chamber, pipe, and auxiliary chamber; R was the specific gas constant.

Similarly, under the impaction of the force F', the force balance (F) generated by the pressure p in the airbag chamber was also determined in Eq. (1). However, the pressure p in Eq. (1) was calculated based on mass rate of air flow Q to airbag chamber as follows:

$$Q = -\frac{d(\rho V)}{dt} = -\rho \dot{V} - rhoV. \quad (12)$$

Based on the general equation between the density and pressure of the air at two different statuses with a polytropic constant of γ expressed by $p_0/\rho_0^\gamma = p/\rho^\gamma$, thus, the ρ and its differential equation were calculated by:

$$\begin{cases} \rho = \rho_0 \Lambda^{-\gamma}; \\ \dot{\rho} = \frac{1}{\gamma R T_0} \Lambda^{\frac{1-\gamma}{\gamma}} \dot{p}; \end{cases} \quad (13)$$

where $\Lambda = p/p_0$; $\rho_0 = p_0/RT_0$.

Replacing Eq. (13) to Eq. (12), the air pressure in the airbag chamber was expressed by the differential equation as:

$$\dot{p} = -\left(p + \gamma R T_0 V_0^{-1} Q\right)\Lambda = -(p + p_0 Q)\Lambda. \quad (14)$$

Similarly, the Q of the air into the auxiliary chamber and the air's density in the auxiliary chamber described by differential equations were also expressed by:

$$\begin{cases} Q = \frac{d(\rho_a V_a)}{dt} = \rho_a \dot{V}_a + \dot{\rho}_a V_a; \\ \dot{\rho}_a = \frac{1}{\gamma R T_0} \Lambda_a^{\frac{1-\gamma}{\gamma}} \dot{p}_a; \end{cases} \quad (15)$$

where $\Lambda_a = p_a/p_0$.

By transforming Eq. (15), the air's pressure in auxiliary chamber described by differential equations had been expressed as:

$$\dot{p}_a = \gamma R T_0 V_{0a}^{-1} \Lambda_a Q = p_0 \Lambda_a Q = p_a Q. \quad (16)$$

With the air's displacement x_p in pipe, Q of the air through the pipe was calculated as:

$$Q = \rho_p A_p \dot{x}_p. \quad (17)$$

Besides, the study results given by Kosenkov, et al.[17] and Robinson,[24] showed that the Q of the air through the pipe was strongly influenced by the section area of the pipe (A_p) and the air pressures in the airbag and auxiliary chambers (p and p_a). Therefore, the Q of the air through the pipe was also calculated via the parameters of A_p, p, and p_a as follows:[17,26]

$$m_p \ddot{x}_p + 0.5 \rho_p A_p \Psi \dot{x}_p^2 \text{sign}(\dot{x}_p) + A_p(p - p_a) = 0; \quad (18)$$

where m_p was defined in Eq. (6); $\Psi = \alpha + 0.886 \beta l_p A_p^{-0.5}$.

According to Darcy formula,[6] the resisting force in pipe's flow in Eq. (18) is defined by:

$$F_p = 0.5 \rho_p A_p \Psi \dot{x}_p^2 \text{sign}(\dot{x}_p); \quad (19)$$

where $\Psi = 0.95$.

By replacing Eq. (17) to Eq. (18), Q of air through the pipe was expressed as:

$$m_p \dot{Q} + 0.5 \Psi Q^2 \text{sign}(Q) + \rho_p A_p^2 (p - p_a) = 0. \quad (20)$$

By combining the equations of the Q of the air into the airbag chamber calculated in Eq. (14), the Q of the air into the auxiliary chamber calculated in Eq. (16), and the Q of the air through the pipe calculated in Eq. (20), the air pressure p in the airbag chamber can be calculated from the AIS's actual design parameters. Therefore, the balancing force of $F = A(p - p_a')$ of Eq. (1) can be also calculated from MFR method.

To calculate the dynamic stiffness parameter k of the AIS, based on the derivative of the F/z, the k was expressed by:[5,6,18,21]

$$k = \frac{dF}{dz} = A\frac{dp}{dz} + (p - p_a')\frac{dA}{dz}; \quad (21)$$

where the air pressure p in the airbag chamber had been calculated by combination of Eqs. (14), (16)–(17), and (20).

Based on the calculation result of dynamic stiffness parameter k of the AIS in Eq. (21), the mathematical model of AIS using the MFR method is described in Fig. 2b.
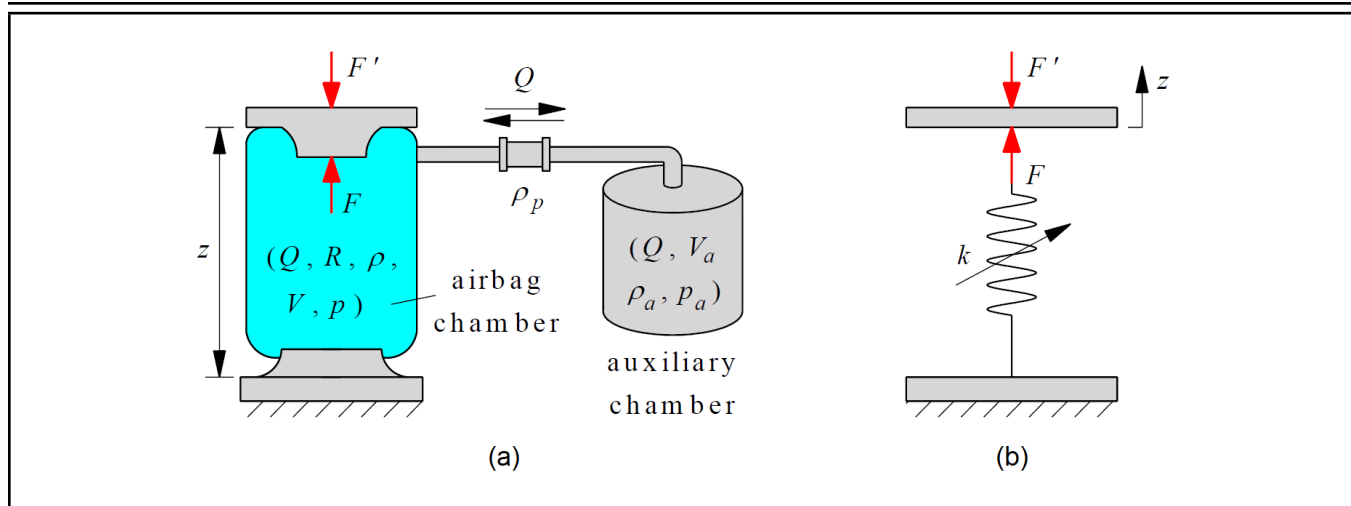
Figure 2. The model of the AIS (a) and MFR of the AIS (b).

Table 1. AIS's operation parameters using the LPM and MFR.

Parameters	Values	Parameters	Values
m / kg	240	V_{0a} / m^3	9.60×10^{-3}
k_s / kN m^{-1}	220.21×10^3	l_p / m	2.5
k_v / kN m^{-1}	150.29×10^3	p_0 / MPa	0.7823
c_δ / kNs m^{-1}	53.332	p_a' / MPa	0.1013
A / m^2	45.2×10^{-3}	ρ_p / kg m^{-3}	9.303
A_p / m^2	0.0785×10^{-3}	T_0 / K	293
V_0 / m^3	14.1×10^{-3}	R / kg K	287.1

3. EXPERIMENTING AND SIMULATING AIR ISOLATION SYSTEM

To determine the accuracy of two methods of the LPM and MFR as well as assess the dynamic characteristic of the AIS using the LPM and MFR, both the experiment and simulation of the AIS were done under a harmonic excitation in a low-frequency range. The AIS's experiment is described in Section 3.1.

3.1. AIS's Experiment and Simulation

To measure the dynamic response of the AIS, the airbag chamber, auxiliary chamber, and piper of the AIS were connected and set up on the MiNG YU machine under the harmonic vibration excitation of the MiNG YU machine with its maximum amplitude (0.03 m) and maximum frequency (15 Hz). The sensors of the force and the displacement of the YMC were set up above and below the airbag chamber to measure the signals of the compression force and the deformation of the airbag chamber and sent to the signal analysis and the display result of YMC. The diagrammatic sketch of the AIS's experimental setup is plotted in Fig. 3.

From AIS's operation parameters provided in Table 1, both the experiment and simulation of the AIS were done in two different cases of: (1) under a harmonic excitation of $q = 6 \times \sin 2\pi f \times t$ mm with its frequency excitation of $f = 0.5$ Hz and (2) under excitation of $q = 3 \times \sin 2\pi f \times t$ mm with its frequency excitation changed from 0.5 to 15 Hz. The measured and simulated result of the force response in the time region, force-deformation characteristic, and dynamic stiffness characteristic in the frequency region of the airbag chamber are shown in Figs. 4a, 4b, and 5.
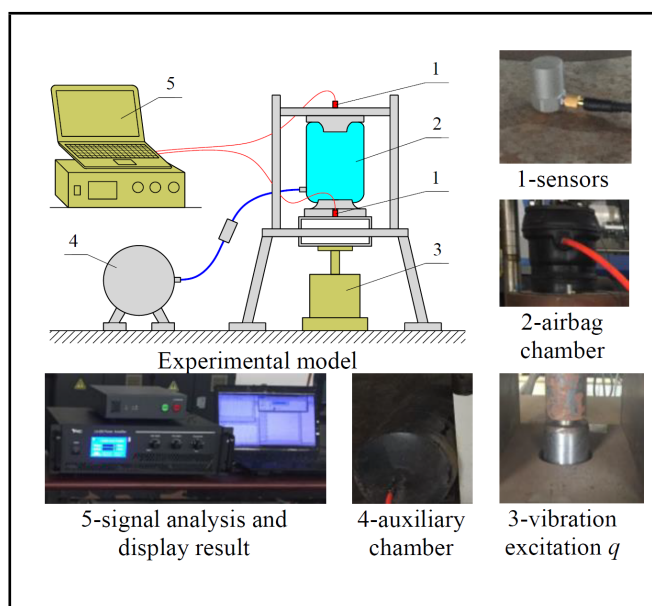

Figure 3. Diagrammatic sketch of the AIS's experiment setup.

3.2. Analysis Results

Case 1: Under the excitation of $q = 6 \times \sin \pi \times t$ mm, the experiment result, and the simulation result of the force response (F) generated by the air pressure in the airbag chamber using the LPM and MFR in Fig. 4a indicates that the curves of the force response with the LPM and MFR are similar. However, the force response of the experiment is significantly delayed in comparison with the force response of the simulation. This could be due to the error of the AIS's operation parameters and the influence of the low-frictional force in airbag's rubber ignored at both calculation and simulation process. However, the difference between the simulation result and the measured result is very small.

Besides, both measured and simulated values of the force-deformation characteristic in airbag chamber plotted in Fig. 4b also show that their curves are the same. Some small errors that appear between experimental and simulation results may also be due to the error influence of the operation parameters and experimental equipment of the AIS. However, the difference between the simulation result and the measured result is also very small. Therefore, the AIS's operation parameters and the
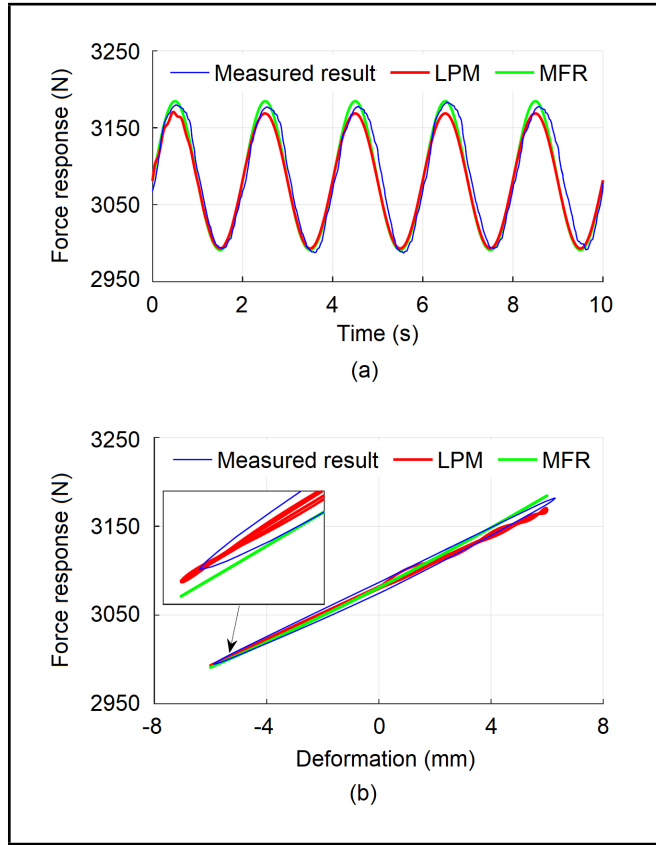
Figure 4. The force response in Case 1 (a) and force-deformation characteristic in Case 1 (b).

Figure 5. The experiment and simulation result of the dynamic stiffness-frequency characteristic of the AIS in Case 2.

two methods of the LPM and MFR could be applied to evaluate the AIS's isolation efficiency.

However, the existing studies on suspension systems using steel springs and air springs indicate that steel spring's dynamics stiffness changes lightly. It isn't affected by the change in the excitation frequencies. Conversely, the air spring's dynamics stiffness has been changed and it is strongly influenced under excited frequencies.[10,11,17,21] Thus, the experiment and simulation of AIS's dynamics stiffness-frequency characteristic under excitation frequencies are also performed in Case 2 to evaluate the stability and accuracy of the two methods of the LPM and MFR.

Case 2: Under the excitation of $q = 3 \times \sin 2\pi f \times t$ mm with its excitation frequency changed from 0.5 to 15 Hz, the dynamic stiffness-frequency characteristic of the AIS between the experiment and the simulation in Fig. 5 shows that the curves of the dynamic stiffness-frequency with the LPM, MFR, and measurement are similar. The result indicates that the dynamic stiffness of the AIS is remarkably influenced by the excitation frequencies. The minimum value of the dynamic stiffness is reached under the excitation range of the frequency from 0.5 to 3.5 Hz while the maximum value of the dynamic stiffness is reached under the excitation range of the frequency from 4 to 7 Hz. This value is similar with the value of numerical simulation in the existing studies.[10,11,21] Therefore, based on measured and simulated values of AIS's dynamics stiffness-frequency characteristic, it further reinforces that both methods of the LPM and MFR could be used to evaluate the AIS's isolation efficiency.

However, with the AIS's mathematical model built based on the LPM method, as shown in Fig. 1b, the influence of
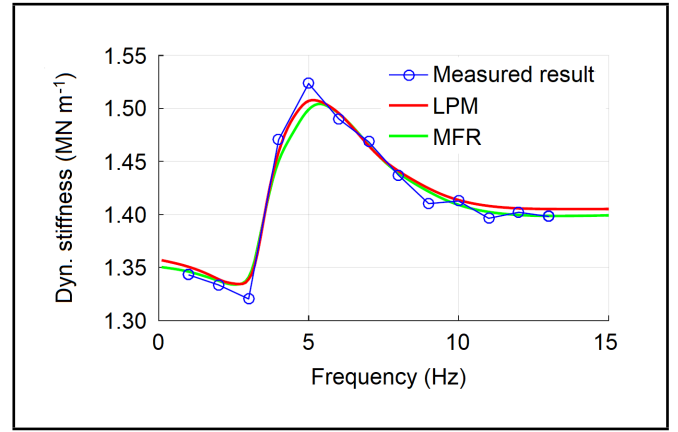
the static stiffness coefficient k_s, viscous stiffness coefficient k_v, damping coefficient c_δ, mass of the air in the pipe m on the AIS's isolation efficiency could be easily evaluated based on the AIS's initial parameters in Eq. (11). In addition, these operation parameters could also be optimized to further enhance the isolation efficiency of the AIS. These issues were performed in the work of Moheyeldein, et al.[6] and Genovese, et al.[7] Thus, this is the advantage of the LPM method. Conversely, with the AIS's mathematical model built based on the MFR method, as shown in Fig. 2b, only AIS's dynamics stiffness in Eq. (21) could be calculated via AIS's original design parameters. Thus, it is difficult to evaluate the influence of the AIS's design parameters on the AIS's isolation efficiency as well as the optimization or control of the AIS, and this is the disadvantage of the MFR method.

Also, the numerical simulation results of the force response, the force-deformation characteristic, and the dynamic stiffness-frequency characteristic in Figs. 4a, 4b, and 5 show that the simulation results with the LPM lightly deviate from the simulation results with the MFR. This can be due to the influence of the damping force (F_p) in the AIS's pipe calculated based on the two different methods of the LPM and MFR as follows.

With the LPM: Based on the values of $m = k^2 m_p$, $m_p = \rho_p A_p l_p$; $c_p = 0.5 A_p \rho_p (c_f + c_e + c_c + c_b)$; $k = AV_{0a}/(V_0 + V_{0a})A_p$; $x = x_p/k$; and $c_\delta = c_p k^{1+\delta}$ with $\delta = 2$ described in Eq. (8) and Eq. (10), these values are then substituted into the viscous force of the pipe in Eq. (9). Equation (9) is transformed and rewritten as:

$$\begin{cases} m_p \ddot{x}_p + F_p + k_v k^{-1}(k^{-1}x_p - z) = 0; \\ F_p = 0.5\rho_p A_p(c_f + c_e + c_c + c_b)\dot{x}_p^2 \text{sign}(\dot{x}_p). \end{cases} \quad (22)$$

With the MFR: The rate of air's mass flow through pipe in Eq. (18) has been also rewritten as:

$$\begin{cases} m_p \ddot{x}_p + F_p + A_p(p - p_A) = 0; \\ F_p = 0.5\rho_p A_p(\alpha + 0.886\beta l_p A_p^{-0.5})\dot{x}_p^2 \text{sign}(\dot{x}_p). \end{cases} \quad (23)$$

where F_p is the resisting force of flow in pipe described in Eq. (19).[17,26]

Because the pipe's viscous force is equivalent to mass of the moving air in same AIS's pipe. This means that Eq. (22) and Eq. (23) are equivalent. Therefore, the damping force (resisting force of flow) in AIS's pipe determined via the LPM and

MFR is rewritten as:

$$F_p = \Gamma \dot{x}_p^2 \text{sign}(\dot{x}_p); \qquad (24)$$

where $\Gamma = \begin{cases} 0.5\rho_p A_p(c_f + c_e + c_c + c_b) & \text{with LPM;} \\ 0.5\rho_p A_p(\alpha + 0.886\beta l_p A_p^{-0.5}) & \text{with MFR.} \end{cases}$

Therefore, the damping force of the pipe with both the LPM and MFR is directly affected by the air density and pipe size. Under the same simulation condition in Case 1, the damping force response of F_p with LPM and MFR is shown in Fig. 6.

The simulation result indicates that the F_p with LPM and MFR has slightly deviated. Thus, it significantly affects the simulation results between the LPM and MFR in Figs. 4a, 4b, and 5.

Besides, Eq. (24) shows that in addition to depending on the pipe area (A_p) and density of air (ρ_p) of pipe, F_p with LPM also depends directly on total loss coefficients in pipe generated by friction, enlargement, contraction, and bends (c_f, c_e, c_c, c_b), while F_p with MFR depends directly on the total pressure drop coefficient ($\alpha + 0.886\beta l_p A_p^{-0.5}$) and the length ($l_p$) of the pipe. Therefore, this is the reason that the LPM is mainly applied to the AIS using the complex pipes[11,12] while the MFR is applied to the AIS using the parallel pipes or long pipes.[2,16] However, the existing studies have not explained this issue in detail.

From analyzed results, we could see that two methods of the LPM and MFR applied to the single dynamic model of the AIS are similar. The error in simulation results between LPM and MFR is very small. Therefore, both methods could be applied to the AIS of vehicles to evaluate vehicle comfort. However, the vehicle's isolation systems are always equipped with multiple AISs, thus, the efficiency and accuracy of the LPM and MFR applied to the multiple AISs of the different vehicles can be affected. To clarify these issues, two different models of the two-axle and multi-axle vehicles using the AISs are researched to further elucidate the isolation efficiency of the AIS using the LPM and MFR.

4. AIS'S EFFICIENCY ON VEHICLE RIDE COMFORT WITH TWO CALCULATION METHODS

4.1. Dynamic Model of Vehicles Using AIS

To evaluate the isolation efficiency and application of the LPM and MFR to the vehicles, two vehicle models including the two-axle automobile model and multi-axle heavy truck model equipped with the AIS were researched. Their dynamic models are plotted in Figs. 7a and 7b.

With the two-axle automobile model in Fig. 7a, z_b, z_{a1}, and z_{a2} were the vehicle's vertical displacement, front-axle of wheel, and rear-axle of wheel; m_b, m_{a1}, and m_{a2} were the mass of the vehicle body, front wheel axle, and rear wheel axle; ϕ_b was the pitching angle of the vehicle body; k_{w1} and k_{w2} were the stiffness parameters of the front and rear wheels; q_1 and q_2 were the vibration excitation of the road surface at the front and rear wheels; F_1 and F_2 were the force responses of the front and rear AIS; l_1 and l_2 were the automobile's length; v_0 was the automobile's speed.

With the four-axle heavy truck model in Fig. 7b, z_c, z_b, and z_{ai2} were the vertical displacement of cabin, vehicle's floor,
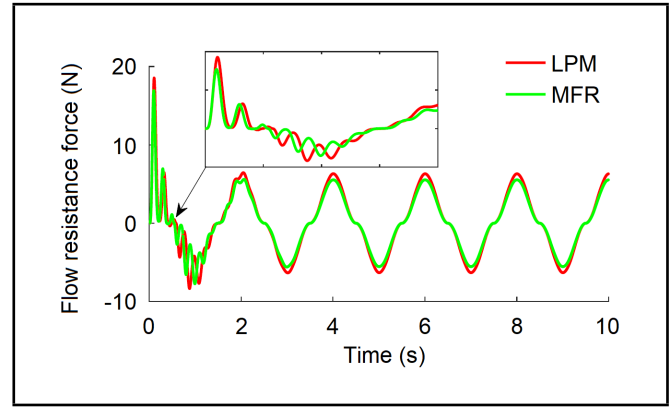

Figure 6. Resisting force of the air flow in AIS's pipe in Case 1.

and wheel-axle; m_c, m_b, and m_{ai} were the mass of cabin, vehicle's floor, and wheel-axles; ϕ_c and ϕ_b were the pitching angle of cabin and vehicle's floor; k_{w1}, k_{w2}, k_{w3}, and k_{w4} were the stiffness parameters at the first wheel, second wheel, third wheel, and fourth wheel; q_1, q_2, q_3, and q_4 were the vibration excitation of the road surface at the first wheel, second wheel, third wheel, and fourth wheel, respectively; F_1, F_2, and F_3 were the force responses of the heavy truck's AIS; l_j and v_0 were the distance and speed of four-axle vehicle ($i = 1, 2, 3$; $j = 1, 2, \ldots, 7$).

Based on lumped parameter models of vehicles in Fig. 7, the motion equations of two-axle and multi-axle vehicles could be written based on Newton's second law and expressed as follows:

$$\mathbf{M}\ddot{\mathbf{Z}}(t) + \mathbf{C}_c\dot{\mathbf{Z}}(t) + \mathbf{K}_c\mathbf{Z}(t) + \mathbf{F}(t) = \mathbf{K}_w\mathbf{Q}(t); \qquad (25)$$

where $\mathbf{Z}(t)$ and $\mathbf{Q}(t)$ were vectors of the displacement and road surface excitation; $\mathbf{M}$ was the mass matrix; $\mathbf{C}_c$ and $\mathbf{K}_c$ were the damping and stiffness matrices of cab's isolations of the multi-axle vehicle; $\mathbf{K}_w$ was the stiffness matrix of wheels; $\mathbf{F}(t)$ was the force response of AIS determined via two methods of LPM and MFR in Sections 2.1 and 2.2.

In the actual condition, both the two-axle and multi-axle vehicles always travelled on the random road surface. Thus, to simulate and analyze the vibration in vehicle's dynamic models, random road surface has been chosen to establish an excitation function q_j of the wheels in the vector of $\mathbf{Q}(t)$. According to ISO 8068[27] and calculated results in existing studies,[4,6,9,28,29] the random road surface at the wheels of vehicles was expressed as:

$$\dot{q}_1 + 2\pi n_0 v_0^2 q_1 = 2\pi n_0 \sqrt{R(n)v_0}\, w; \qquad (26)$$

$$\begin{cases} q_2 = q_1[t + (l_1 + l_2)/v_0], & \text{Two-axle vehicle;} \\ \begin{cases} q_2 = q_1[t + l_3/v_0], \\ q_3 = q_2[t + (l_4 + l_5)/v_0], & \text{Four-axle vehicle;} \\ q_4 = q_3[t + (l_6 + l_7)/v_0], \end{cases} \end{cases}$$

where $R(n) = R(n_0)(n^2/n_0^2)$; n was the space frequency; $n_0 = 0.1$ 1/m; $R(n_0)$ was power spectral density of random road; w was the white noise signal; and v_0 was the moving speed of the vehicle.

Based on ISO 8068,[27] the medium roughness of the road surface in ISO level B with $R(n_0) = 64 \times 10^{-6}$ m^3 was used to establish the vibration excitation of q1 in the condition of the
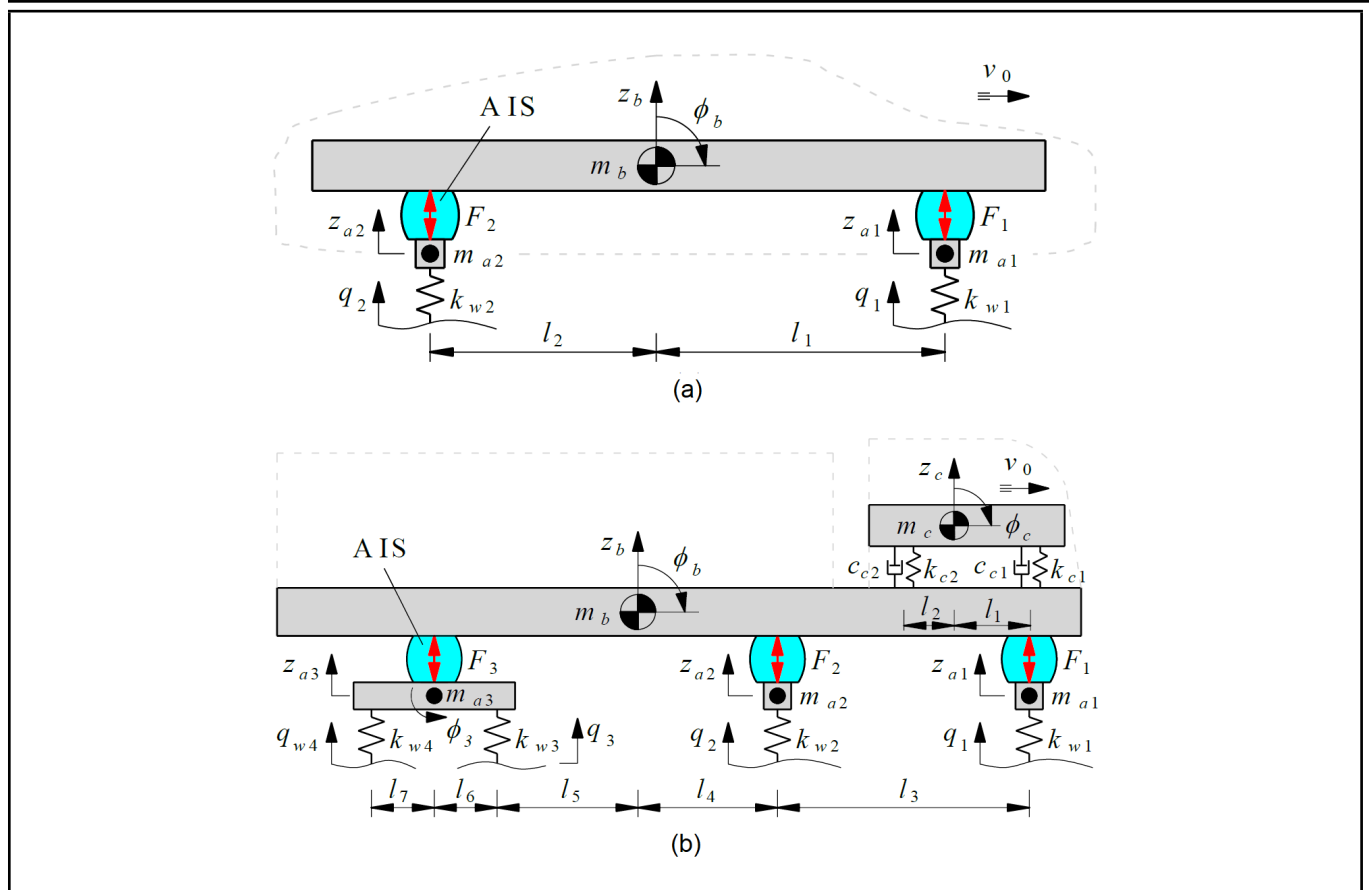
Figure 7. Lumped parameter model of two-axle automobile (a) and four-axle heavy truck (b).
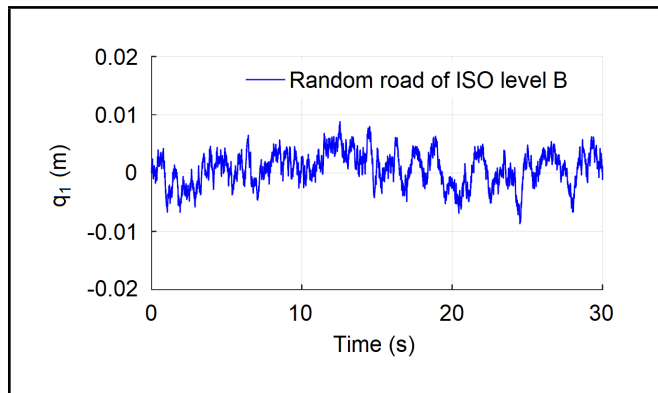

Figure 8. The medium road surface roughness of ISO level B.

vehicle moving a speed $v_0 = 20$ m s^{-1}. The q_1 is simulated and plotted in Fig. 8. This road surface excitation was then applied to evaluate the isolation efficiency of the AIS using the LPM and MFR.

4.2. Evaluation Criteria

In the existing studies of vehicle isolation systems, the deformation of the isolation system, the vehicle's ride quality, and the road friendliness were directly applied to evaluate the isolation efficiency of the isolation systems,[11,28,30–36] especially the two indexes of the road-friendliness and ride quality.

With ride quality index: Vehicle's root-mean-square (RMS) acceleration was applied to evaluate the vehicle ride quality.[9,29,32,35–37] According to ISO 2631-1,[32] the expression of the RMS acceleration of the vehicle dynamic models in Fig. 7

was expressed as:

$$a_{w\chi} = \sqrt{\frac{1}{T} \int_0^T a_\chi^2(t) dt};\qquad(27)$$

where subscript χ referred to the z_b and ϕ_b with the two-axle automobile and the z_c and ϕ_c with the four-axle heavy truck; $a_\chi(t)$ was acceleration responses in the translational and rotational directions of two-axle automobile and four-axle heavy truck depending on time of T.

The $a_{w\chi}$ was then applied to assess the isolation efficiency of the AIS using the LPM and MFR on ameliorating the comfort of two-axle automobile and four-axle heavy truck.

With road friendliness index: When the heavy truck was traveling on the road, the wheel dynamic loads had a great impact on the road damage, especially at the high moving speed of the vehicle on the poor road surface.[30,31,33,34] Effect of wheel's dynamic load to road-friendliness of the vehicles was evaluated via the dynamic load coefficient (DLC) as:[30,34]

$$\text{DLC}_j = \frac{F_{wj,\text{RMS}}}{F_{wj}};\qquad(28)$$

where $F_{wj,\text{RMS}}$ was the RMS dynamic load of the wheels of the two-axle automobile ($j = 1 - 2$) and four-axle heavy truck ($j = 1 - 4$); F_{wj} represented the static loads at wheel-axles j.

The DLC was also applied to assess the isolation efficiency of the AIS using the LPM and MFR on improving the road friendliness of the two-axle automobile and four-axle heavy truck. Therefore, the smaller values of $a_{w\chi}$ and DLC_j mean to be the better isolation efficiency of the AIS using the corresponding method.

Table 2. The operation parameters of an automobile.

Parameters	Values	Parameters	Values
m_b / kg	1450	c_1 / kNs m^{-1}	1.45
m_{a1} / kg	66	c_2 / kNs m^{-1}	1.50
m_{a2} / kg	78	l_1 / m	1.40
$k_{w1,2}$ / kN m^{-1}	201	l_2 / m	1.60

4.3. Results and Discussions

4.3.1. Comparative efficiency between LPM and MFR on two-axle automobile

The moving speed of the vehicles greatly affected the ride comfort and road friendliness.[29,37–40] Thus, to evaluate the isolation efficiency of the AIS using the LPM and MFR on improving road-friendliness and comfort in two-axle automobile, from operation parameters of the two-axle automobile listed in Table 2,[25,39] a vehicle's speed range from 2.5 to 40 m s^{-1} is simulated at a vibration excitation q_1 in Fig. 8. Results have been plotted in Fig. 9.

The simulation result in Fig. 9 indicates that all RMS accelerations in both vertical vibration and pitching angle of the automobile body (a_{wb} and $a_{w\phi b}$) and DLC at wheel-axle are strongly increased when the vehicle's moving speed is increased and vice versa. This means that both comfort and road-friendliness in two-axle automobile are significantly reduced when the vehicle is moving in the high-speed region over 25 m s^{-1}. This result is like the result in the existing studies.[37–39]

When the AIS using the LPM and MFR is applied on the two-axle automobile, the results in Fig. 9 show that both the a_{wb} and $a_{w\phi b}$; and the DLC with the MFR are smaller than that of the LPM under the different speeds. This implies that using the MFR method for the AIS of two-axle automobiles, the comfort and road-friendliness in two-axle vehicle obtained are better than that of the LPM method. This is due to the influence of the AIS with the parallel pipes or long pipes equipped on the two-axle automobiles.[2,16,39,40] Therefore, the MFR method should be used for designing and evaluating isolation efficiency of AIS for two-axle automobiles. This is the reason that the MFR method is always applied to evaluate the ride comfort of two-axle automobiles including ambulances and cars.[24,25,40] However, the existing studies have not clarified this issue.

4.3.2. Comparative efficiency between LPM and MFR on multi-axle heavy truck

Similarly, to evaluate the isolation efficiency of the AIS using the LPM and MFR on improving both comfort and road-friendliness in multi-axle truck, from operation parameters of the four-axle heavy truck provided in Table 3,[41,42] a speed region from 2.5 to 30 m s^{-1} of vehicle is also simulated under the road surface roughness in Fig. 8. Results of comfort and road-friendliness are shown in Figs. 10 and 11.

With heavy truck's comfort: Fig. 10 indicates that RMS acceleration of both vertical vibration and pitching angle in cab (a_{wc} and $a_{w\phi c}$) are also remarkably increased with the increase of the vehicle's speed and vice versa. This means that the ride comfort of the heavy truck is also significantly decreased when the vehicle's speed is increased. At low-speed region below 10 m s^{-1}, both the values of a_{wc} and $a_{w\phi c}$ with the MFR are lower than that of the LPM. Conversely, at a speed region over
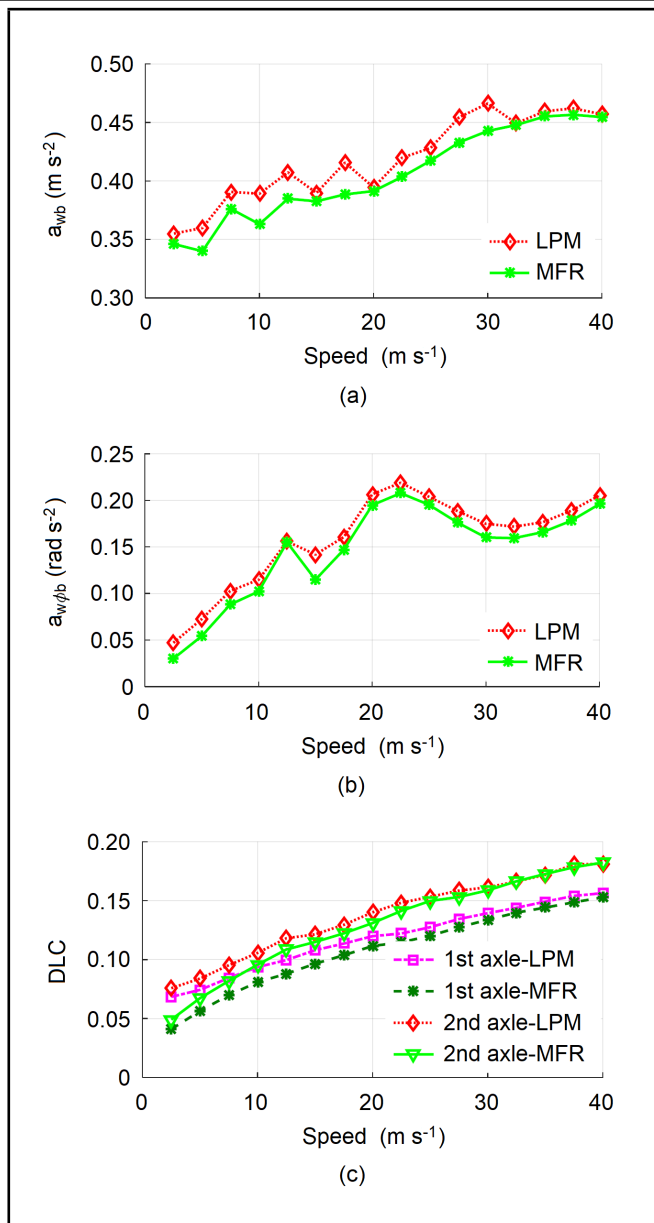

Figure 9. Simulation result of two-axle automobile under various speeds, vertical RMS acceleration (a), RMS pitching acceleration (b), and DLC at wheel axles (c).

12.5 m s^{-1}, both these values with the LPM are lower than that of the MFR. This means that with the multi-axle heavy truck using the AIS, the ride comfort of the vehicle obtained by the LPM method is better than that of the MFR method. Also, in the actual condition, the heavy trucks mainly moved at the speed region of 10 to 20 m s^{-1}.[30,33,41,42] Thus, the LPM method should be used for designing and assessing the isolation efficiency of the AIS equipped on multi-axle heavy trucks to better improve ride comfort.

With road friendliness of truck: The simulation result of DLC in Fig. 11a shows that DLC at wheel-axles is significantly increased with the increase of the vehicle's speed. Besides, DLC at 3rd wheel-axle is higher than that of 2nd and 4th wheel-axles, while DLC at 1st wheel axle is the smallest. This means that the effect of 3rd wheel axle on the damage of the road surface is greatest, especially in the high-speed region of the vehicle over 20 m s^{-1}. To compare the efficiency of the LPM and MFR in improving road-friendliness of the

Table 3. The operation parameters of a heavy truck.

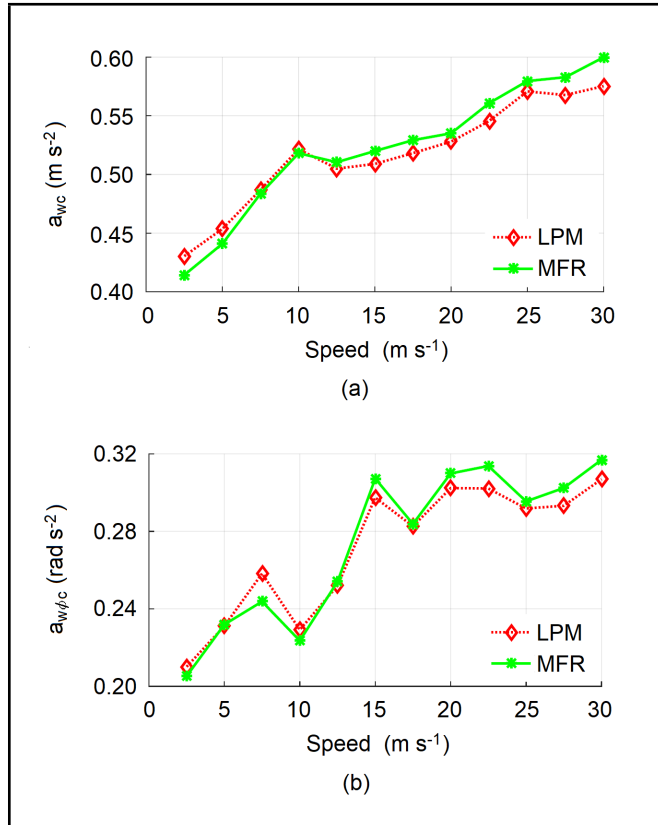| Parameters	Values	Parameters	Values
m_c / kg	500	c_3 / kN m^{-1}	24.1
m_b / kg	19000	k_{w1} / MN m^{-1}	0.69
m_{a1} / kg	450	$k_{w2,3,4}$ / MN m^{-1}	1.38
m_{a2} / kg	1025	l_1 / m	1.10
m_{a3} / kg	1314	l_2 / m	1.00
$c_{c1,2}$ / kNs m^{-1}1	0.20	l_3 / m	2.50
$k_{c1,2}$ / kN m^{-1}	100	l_4 / m	2.18
c_1 / kN m^{-1}	7.03	l_5 / m	1.37
c_2 /kN m^{-1}	24.1	$l_{6,7}$ / m	0.75

Figure 10. Simulation result of four-axle heavy truck under various speeds, vertical RMS acceleration (a) and RMS pitching acceleration of the cab (b).

Figure 11. Simulation result of four-axle heavy truck under various speeds, DLC at wheel axles with LPM (a) and DLC at first and third wheel axles with LPM and MFR (b).

ride comfort and the road friendliness of the multi-axle heavy truck with the LPM are better than that of the MFR. Therefore, to enhance the ride comfort and the road friendliness of the vehicles as well as optimize the isolation efficiency of the AIS, in the design and calculation process of the AIS for the vehicles, the MFR method should be applied for the AIS of two-axle automobiles while the LPM method should be applied for the AIS of multi-axle vehicles.

5. CONCLUSIONS

The numerical simulation and experiment of the AIS is given to assess the accuracy of the two methods of the LPM and MFR. The effect of the AIS using the LPM and MFR on both comfort and road-friendliness in vehicles is then evaluated via two-axle and multi-axle vehicles. The results of the study are summarized as follows:

(1) By using the single model of the AIS, the simulation and experiment results of the force response, force-deformation characteristic, and dynamic stiffness-frequency characteristic of the AIS with two methods of the LPM and MFR are similar. Therefore, both methods could be used for AIS in vehicles to evaluate vehicle's comfort.

(2) By applying the AIS on the two-axle and multi-axle vehicles to ameliorate both comfort and road-friendliness, simulation results indicate that the MFR method improves both comfort and road-friendliness in two-axle automobile better than that the LPM, while the LPM method improves both comfort and road-friendliness in multi-axle

truck, DLC at 1st and 3rd wheel-axles with the LPM and MFR has been compared in Fig. 11b. The result revealed that DLC at 1st and 3rd wheel-axles with LPM is reduced compared to MFR under all different speeds. This is due to the influence of AIS with the complex pipes equipped on the multi-axle heavy trucks.[11,12] Therefore, the road friendliness of the heavy truck obtained by using the LPM is better than that of the MFR, and the LPM method should be applied for designing and evaluating the isolation efficiency of the AIS of multi-axle heavy trucks to better ameliorate the road friendliness. Thus, this is also the reason that the AIS's dynamic model of multi-axle vehicles including trains, heavy trucks, and tractor trucks mainly applied the LPM method to design and improve the comfort and road-friendliness.[1,5,22] However, the existing studies have not also clarified the reason that the LPM method should be applied for the AIS of the multi-axle vehicles.

Based on the analysis and comparison results of the LPM and MFR used on the two-axle automobile and multi-axle heavy truck in Sections 4.3.1 and 4.3.2, we can see that the ride comfort and the road friendliness of the two-axle automobile with the MFR are better than that of the LPM; whereas the
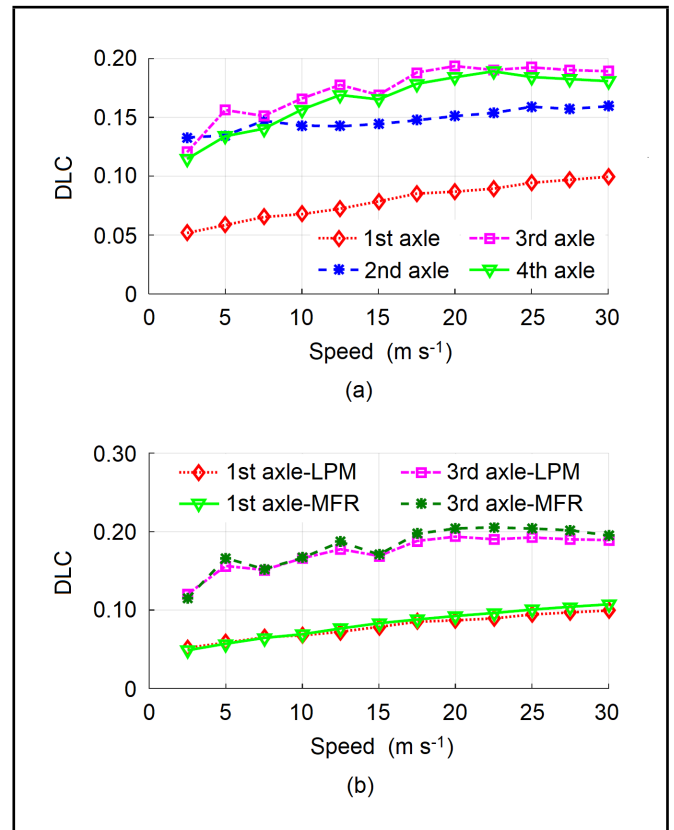
heavy truck better than the MFR. Thus, the MFR should be applied to the AIS of two-axle vehicles while the LPM should be applied to the AIS of multi-axle vehicles.

(3) The MFR method should be applied to the AIS designed by the parallel pipes or long pipes whereas the LPM method should be used to the AIS designed by the complex pipes to more accurately assess the isolation efficiency of the AIS in improving both comfort and road-friendliness in vehicles.

(4) This study has elucidated the efficiency and application range of two methods of the LPM and MFR of the AIS while the existing studies have not explained this issue in detail.

ACKNOWLEDGEMENTS

REFERENCES

[1] Presthus, M. *Derivation of air spring model parameters for train simulation*, Lulea University of Technology, (2002).

[2] Docquier, N., Fisette, P., and Jeanmart, H. Multiphysic modelling of railway vehicles equipped with pneumatic suspensions, *Vehicle System Dynamic*, **45**, 505–524, (2007).

[3] Xie, Z., Wong, P., Zhao, J., Xu, T., Wong, K. I., and Wong, H. C. A noise-insensitive semi-active air suspension for heavy-duty vehicles with an integrated fuzzy-wheelbase preview control, *Mathematical Problems in Engineering*, **2013**, 1–12, (2013). https://doi.org/10.1155/2013/121953

[4] Zha, J., Zhang, J., and Nguyen, V. Comparison of vibration isolation performance of seat suspension with three various design modes, (in Chinese), *Journal of Southeast University*, **38**, 363–372, (2022). https://doi.org/10.3969/j.issn.1003-7985.2022.04.005

[5] da Silva Bravo, R. R., de Cantuaria Gama, A. T., Oliveira, A. A. M., and De Negri, V. J. Component sizing and sensitivity analysis of design parameters of a hydraulic-pneumatic regenerative braking system for heavy duty vehicles, *Energy*, **264**, 126021, (2023). https://doi.org/10.1016/j.energy.2022.126021

[6] Moheyeldein, M. M., Abd-El-Tawwab, A. M., Abd Elgwwad, K. A., and Salem, M. M. M. An analytical study of the performance indices of air spring suspensions over the passive suspension, *Beni-Suef University Journal of Basic and Applied Sciences*, **7**, 525–534, (2018). https://doi.org/10.1016/j.bjbas.2018.06.004

[7] Genovese, A., Strano, S., and Terzo, M. Design and multi-physics optimization of an energy harvesting system integrated in a pneumatic suspension, *Mechatronics*, **69**, 102395, (2020). https://doi.org/10.1016/j.mechatronics.2020.102395

[8] Zhu, H., Yang, J., and Zhang, Y. Modeling and optimization for pneumatically pitch interconnected suspensions of a vehicle, *Journal of Sound and Vibration*, **432**, 290–309, (2018). https://doi.org/10.1016/j.jsv.2018.06.043

[9] Zhang, L., Nguyen, V., Wang, C., Xu, S., and Li, H. Review research on isolation systems of the cab and driver's seat in soil compactors, *SAE International Journal of Vehicle Dynamics, Stability, and NVH*, **7**, 115–136, (2023). https://doi.org/10.4271/10-07-02-0008

[10] Ni, D., Nguyen, V., and Li, S. Performance analysis of the seat suspension using different models of the optimal negative-stiffness-structures, *Proc. IMechE, Part D: Journal of Automobile Engineering*, **237**, 1313–1326, (2023). https://doi.org/10.1177/09544070221091040

[11] Berg, M. A non-linear rubber spring model for rail vehicle dynamics analysis, *Vehicle System Dynamics*, **30**, 197–212, (1998). https://doi.org/10.1080/00423119808969447

[12] Berg, M. A three-dimensional air spring model with friction and orifice damping, *Vehicle System Dynamics*, **33**, 528–539, (1999). https://doi.org/10.1080/00423114.1999.12063109

[13] Makaryants, G. and Shkhmatov, E. Experimental study of active pneumatic vibration isolation system, *Engineering*, **2018**, 220860532, (2018).

[14] Zhu, H., Yang, J., Zhang, Y., and Feng, X. A novel air spring dynamic model with pneumatic thermodynamics, effective friction and viscoelastic damping, *Journal of Sound and Vibration*, **408**, 87–104, (2017). https://doi.org/10.1016/j.jsv.2017.07.015

[15] Zhu, H., Yang, J., and Zhang, Y. Dual-chamber pneumatically interconnected suspension: Modeling and theoretical analysis, *Mechanical Systems and Signal Processing*, **147**, 107125, (2021). https://doi.org/10.1016/j.ymssp.2020.107125

[16] Nieto, A., Morales, A., Chicharro, J., and Pintado, P. Unbalanced machinery vibration isolation with a semi-active pneumatic suspension, *Journal of Sound and Vibration*, **329**, 3–12, (2010). https://doi.org/10.1016/j.jsv.2009.09.001

[17] Kosenkov, P. V. and Makaryants, G. M. Control algorithm design of the active pneumatic vibration isolator, *Procedia Engineering*, **176**, 653–660, (2017). https://doi.org/10.1016/j.proeng.2017.02.309

[18] Zhu, H., Yang, J., Zhang, Y., Feng, X., and Ma, Z. Nonlinear dynamic model of air spring with a damper for vehicle ride comfort, *Nonlinear Dynamics*, **89**, 1545--1568, (2017). https://doi.org/10.1007/s11071-017-3535-9

[19] Zhou, H., Nguyen, V., and Wu, X. Performance of the CHPI on improving vibration of vibratory roller cab: experiment and simulation, *Noise & Vibration Worldwide*, **52**, 102–112, (2021). https://doi.org/10.1177/0957456521999837

20 Xu, S., Nguyen, V., Li, S., and Ni, D. Performance of the machine learning on controlling the pneumatic suspension of automobiles on the rigid and off-road surfaces, *SAE International Journal of Passenger Vehicle Systems*, **15**, 169–182, (2022). https://doi.org/10.4271/15-15-03-0012

21 Ryaboy, V. M. Static and dynamic stability of pneumatic vibration isolators and systems of isolators, *Journal of Sound and Vibration*, **333**, 31–51, (2014). https://doi.org/10.1016/j.jsv.2013.06.034

22 Sundvall, P. Comparisons between predicted and measured ride comfort in trains—a case study on modeling, TRITAFKT Report, Division of Railway Technology, Department of Vehicle Engineering, Royal Institute of Technology, Stockholm, Sweden, (2001).

23 Razenberg, J. *Modelling of the hydro-pneumatic suspension system of a rally truck*, Eindhoven University of Technology, (2009).

24 Robinson, W. *A pneumatic semi-active control methodology for vibration control of air spring based suspension systems*, Iowa State University, (2012).

25 Li, S., Li, H., Zhang, L., and Wang, X. A comparative study of isolation performance of electric automobile seat's suspension added by negative-stiffness structure models, *Noise & Vibration Worldwide*, **54**, 81–91, (2023). https://doi.org/10.1177/09574565231154242

26 Alonso, A., Giménez, J., Nieto, J., Vinolas, J. Air suspension characterisation and effectiveness of a variable area orifice, *Vehicle System Dynamics*, **48**, 271–286, (2010). https://doi.org/10.1080/00423111003731258

27 ISO 8068 Mechanical vibration—Road surface profiles—Reporting of measured data: General requirements, International Organization for Standardization, Geneve, Switzerland, (1995).

28 Jiang, J., Min, L., Jing, Y., Ding, S., Yu, M., and Jie, W. Improving ride comfort of a soil compactor based on the NSS embedded into the seat's semiactive suspension, *International Journal of Acoustics and Vibration*, **28**, 117–129, (2023). https://doi.org/10.20855/ijav.2023.28.11931

29 Xiu, Y., Wang, X., Li, H., Lu, W., Nguyen, V., Jiang, J., and Li, S. Comparative vibration isolation assessment of two seat suspension models with different negative stiffness structure, *SAE International Journal of Vehicle Dynamics, Stability, and NVH*, **7**, 99–112, (2023). https://doi.org/10.4271/10-07-01-0007

30 Kulakowski, B., Husted, D., and Streit, D. Models of dynamic load coefficient for a two-axle truck obtained from road simulator data, *Heavy Vehicle System, International Journal of Heavy Vehicle Design*, **3**, 293–305, (1996). https://doi.org/10.1504/IJHVS.1996.054566

31 Cole, D. and Cebon, D. Truck suspension design to minimize road damage, *Proc. IMechE, Part D: Journal of Automobile Engineering*, **210**, 95–107, (1996). https://doi.org/10.1243/pime_proc_1996_210_251_02

32 ISO 2631-1 Mechanical vibration and shock—Evaluation of human exposure to whole body vibration—Part 2: General requirements, International Organization for Standardization, Geneve, Switzerland (1997).

33 Lu, Y., Yang, S., Li, S., and Chen, L. Numerical and experimental investigation on stochastic dynamic load of a heavy duty vehicle, *Applied Mathematical Modelling*, **34**, 2698–2710, (2010). https://doi.org/10.1016/j.apm.2009.12.006

34 Buhari, R., Rohani, M., and Abdullah, M. Dynamic load coefficient of tyre forces from truck axles, *Applied Mechanics and Materials*, **405–408**, 1900–1911, (2013). https://doi.org/10.4028/www.scientific.net/amm.405-408.1900

35 Wang, S., Nguyen, V., Zhou, H., and Wang, C. Improving ride comfort in vehicles with seat vibration isolator embedded by different negative stiffness models, *SAE International Journal of Passenger Vehicle Systems*, **15**, 205–222, (2022). https://doi.org/10.4271/15-15-03-0015

36 Jiang, J., Guo, X., Li, L., Nguyen, V., Li, S., and Chen, C. Analysis of the effect of three different dynamic models embedded into the seat suspension system on the ride performance of a vibratory roller, *SAE International Journal of Vehicle Dynamics, Stability, and NVH*, **6**, 297–310, (2022). https://doi.org/10.4271/10-06-03-0020

37 Yang, J., Nguyen, V., Wang, X., Lu, J., Shi, D., and Ma, C. Performance study of semi-active seat suspension added by quasi-zero stiffness structure under various vibratory roller models, *Proc. IMechE, Part D: Journal of Automobile Engineering*, **237**, 1–15, (2023). https://doi.org/10.1177/09544070221143167

38 Zhou, G., Ma, H., Wang, Y., and Cao, S. Vehicle velocity optimization for ride comfort improvement of automated driving in speed hump conditions, *IFAC—PapersOnLine*, **54**, 410–417, (2021). https://doi.org/10.1016/j.ifacol.2021.10.197

39 Xu, S., Nguyen, V., Li, S., and Ni, D. Performance of the machine learning on controlling the pneumatic suspension of automobiles on the rigid and off-road surfaces, *SAE International Journal of Passenger Vehicle Systems*, **15**, 169-–182, (2022). https://doi.org/10.4271/15-15-03-0012

40 Xu, S., Zhang, J., and Nguyen, V. Applying machine learning for car's semi-active air suspension under soft and rigid roads, (in Chinese), *Journal of Southeast University*, **38**, 300–308, (2022). https://doi.org/10.3969/j.issn.1003-7985.2022.03.012

41 Li, B. *3-D Dynamic modeling and simulation of a multi-degree of freedom 3-axle rigid truck with trailing arm bogie suspension*, New South Wales, Australia: University of Wollongong, (2006).

42 Tsampardoukas, G., Stammers, C., and Guglielmino, E. Hybrid balance control of a magnetorheological truck suspension, *Journal of Sound and Vibration*, **317**, 514–536, (2008). https://doi.org/10.1016/j.jsv.2008.03.040